

Article

# A Modified Johnson-Cook Model for Hot Deformation Behavior of 35CrMo Steel

Sanxing Wang <sup>1</sup>, Yuanchun Huang <sup>1,2,\*</sup>, Zhengbing Xiao <sup>1,2</sup> , Yu Liu <sup>2</sup> and Hui Liu <sup>2</sup>

<sup>1</sup> College of Mechanical and Electrical Engineering, Central South University, Changsha 410083, China; wangsanxing@csu.edu.cn (S.W.); xiaozb@csu.edu.cn (Z.X.)

<sup>2</sup> Light Alloy Research Institute, Central South University, Changsha 410012, China; csuliuyu@csu.edu.cn (Y.L.); liuhui2015@csu.edu.cn (H.L.)

\* Correspondence: science@csu.edu.cn; Tel.: +86-0731-8887-6315

Received: 20 June 2017; Accepted: 23 August 2017; Published: 1 September 2017

**Abstract:** In this work, a compression experiment of 35CrMo steel is carried out over a wide range of temperatures (1123–1423 K) and strain rates (0.1–10 s<sup>-1</sup>) to obtain further understandings of the flow behaviors. The results show that the strain hardening effect of 35CrMo steel is stronger than that of dynamic recrystallization at low temperature and high strain rate; on the contrary, the rheological curves show typical dynamic recrystallization characteristics at high temperature and low strain rate. This indicates that the strain hardening and recrystallization behavior of 35CrMo steel is affected by temperature, strain and strain rate, and its true stress-strain curves can be observed typical work hardening and dynamic softening features. A modified Johnson-Cook (JC) model is developed to predict the flow stress of the alloy. The results of the comparison show that the predicted values of the modified JC model are in good agreement with the experimental values.

**Keywords:** 35CrMo steel; constitutive equation; hot deformation; strain hardening

## 1. Introduction

35CrMo steel has been widely used in the manufacture of various large components and medium-sized parts, such as driveshafts, crankshafts, and fasteners, for its excellent characteristics of good wear, impact, fatigue, and corrosion resistance [1–5]. Service in the deep sea environment of the bearing part and rotary shaft, it is not only subjected to strong alternating loads, but also faces the cross-effect of various corrosion modes, and its corrosion resistance is directly related to the microstructure, which can be effectively controlled by a hot working process [6,7]. Therefore, in order to achieve the excellent properties of 35CrMo steel parts, it is necessary to study its hot deformation behavior in depth.

In order to effectively predict the high temperature flow stress of alloys and metals, researchers put forward different kinds of constitutive equation, which can be divided into phenomenological constitutive models, artificial neural network models, and physics-based models. Johnson-Cook (JC) model [8,9], Arrhenius model [10,11], and L-parameter compensation model [12] proposed by Lin et al., or modified models based on these models, are phenomenological classes. Among them, Arrhenius hyperbolic sine equation is one of the most commonly used constitutive models. In recent years, Arrhenius model and its modified equation were developed to predict the flow behaviors of cast A356 aluminum alloy [13], GCr15 steel [14], AISI 321 austenitic stainless steel [15], 21Cr economical duplex stainless steel [16], Inconel 600 superalloy [17], and 9Cr-1Mo steel [18]. Moreover, neural network models were used to predict the flow behaviors of 28CrMnMoV steel [19], glass fiber reinforced polymers [20], A356 aluminum alloy [21], and 42CrMo steel [22]. In addition, dynamic recrystallization (DRX) model [23], Zerilli-Amstrong (ZA) model [24,25], mechanical threshold stress plasticity (MTS) model [26], Cellular Automata (CA) model [27], and Bonder-Partom (BP) model [28] belong to the

physics-based models. The study of V-4Cr-4Ti [29], medium carbon and vanadium microalloyed steels [30], and Mg-Al-Zn alloy [31] shows that the constitutive equation based on microscopic mechanism has good applicability, which can be used to characterize the relationship between flow stress and microstructure during high-temperature rheological process.

However, these physics-based models, including the DRX model, ZA model, MTS model, and BP model, etc., are mainly based on dislocation theory and kinetics of slip. They always have complex forms and the practical applications are limited, for a large number of experimental data are needed. As one of the empirical models, JC model was widely used with simple expression and only five material constants, and the strain rate hardening and thermal softening effect are taken into account [32,33]. Considering the interaction of temperature, strain and strain rate on the alloys flow stress of 30Cr2Ni4MoV rotor steel and a typical high-strength alloy steel, Wang et al. [34] and Lin et al. [35] have made appropriate changes to the original JC model to describe the flow stress responses of the alloys under different hot deformation conditions. In the modified models, the JC model parameters are often expressed as a function of strain, strain rate, and temperature. For example, some modified JC models were improved to predict flow stresses of 20CrMo alloy steel [36], titanium matrix composites [37], and B1500HS boron steel [38]. Also, the improved JC model has been widely used in a variety of engineering applications, and embedded in a number of finite element software [39–41].

Although some materials have made progress in these constitutive models, there is no research on the JC model of 35CrMo steel in addition to the ZA model under high temperature dynamic compression tests [42,43], and it is unclear whether the existing constitutive model is suitable for describing the relationship between flow stress and hot deformation conditions. Therefore, it is necessary to further study the applicability of the JC model to 35CrMo steel within a certain temperature and strain rate range.

## 2. Experiments and Results

A commercial 35CrMo steel with the composition 0.34C–0.21Si–0.56Mn–0.95Cr–0.19Mo–0.0051S–0.019Si–(balance) Fe (wt %) was used in this investigation. Cylindrical specimens were machined with a diameter of 10 mm and a height of 12 mm. The compression tests were performed on a Gleeble 3810 thermo-simulation machine (Central South University, Changsha, China) in the temperatures range of 1123–1423 K at an interval of 100 K, while the imposed constant strain rates were 0.1, 1, and 10 s<sup>−1</sup>. All specimens were heated up to 1523 K at a heating rate of 10 K/s by thermo-coupled feedback-controlled AC current, and held for 360 s, then cooled to the deformation temperature at a rate of 10 K/s. Prior to the compression test, the sample was held at the deformation temperature for 120 s to eliminate thermal gradients. The reduction in height was 60% at the end of the compression tests. In addition, it should be noted that tests at strain rates exceeding 1 s<sup>−1</sup> will be adiabatic in nature [44]. Stress levels are high enough—even at the highest temperatures—to introduce adiabatic heating. Thus, temperatures will not be constant, and this effect was ignored in this experiment.

It can be seen from the Figure 1 that the true stress-strain curves of 35CrMo steel exhibit peak stresses at small strains, after them the flow stresses decrease monotonically until high strains, and finally stabilized, showing typical work hardening and dynamic softening features under different deformation conditions, respectively. The strain hardening effect of 35CrMo steel is stronger than the dynamic recrystallization softening effect when the temperature is low and the strain rate is high, and the flow stress increases with the increase of strain, such as in 1123 K/0.1 s<sup>−1</sup> and 1323 K/10 s<sup>−1</sup>. On the contrary, at high temperature and low strain rate, the stress increased rapidly to the peak after a slight decline, and followed by a steady state flow. This indicates that the strain hardening and recrystallization behavior of 35CrMo steel is affected by temperature, strain, and strain rate. Although the initial strain value of the curves entering the steady state rheological stage varies with the experimental conditions, most of the curves enter the steady stage after the true strain exceeds 0.25. This phenomenon is the result of dynamic equilibrium between work hardening and various softening mechanisms (dynamic recrystallization, dynamic recovery) [45,46]. As the JC model mainly describes

the relationship between flow stress and temperature, strain, and strain rate in the steady-state rheological stage. Therefore, we intercept the data in Figure 1 where the true strain in the range of 0.25 to 0.6 as the data source of the constitutive equation.

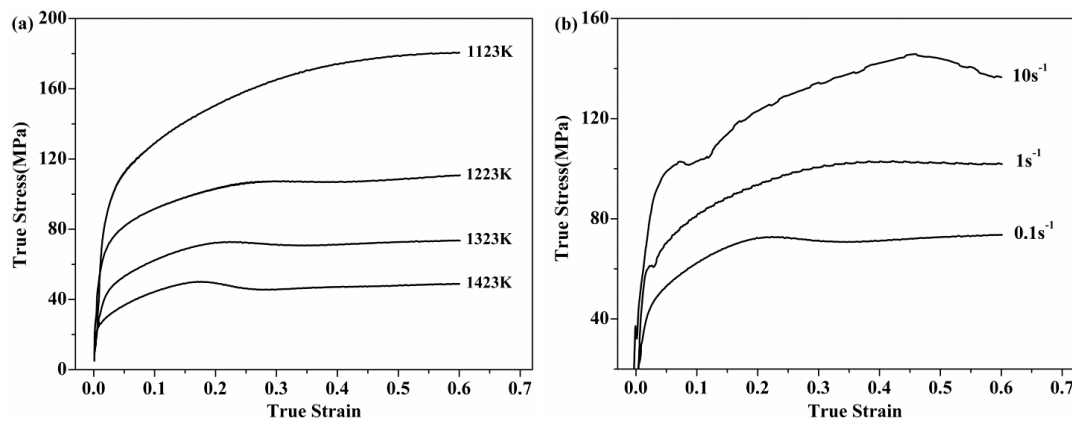


Figure 1. True stress-strain curves of 35CrMo steel; (a) strain rate  $\dot{\epsilon} = 0.1 \text{ s}^{-1}$ ; (b)  $T = 1323 \text{ K}$ .

### 3. The Original JC Model and Its Modified Equation

The original JC model is a purely empirical model. It is well known as a strain, strain rate, and deformation temperature-dependent phenomenological flow stress model, which simple in form and have a clear physical interpretation. The form of original JC model [8,9] can be expressed as:

$$\sigma = (A + B\epsilon^n) \left(1 + C \ln \dot{\epsilon}^*\right) (1 - T^{*m}) \quad (1)$$

where  $\sigma$  is the Von Mises flow stress, MPa;  $A$  is the yield stress at reference strain rate and reference temperature, MPa;  $B$  is the coefficient of strain;  $\epsilon$  is the equivalent plastic strain;  $n$  is the strain hardening exponent;  $C$  and  $m$  are the JC model parameters which represent the coefficient of strain rate sensitivity and thermal softening exponent, respectively.  $\dot{\epsilon}^* = \dot{\epsilon}/\dot{\epsilon}_0$  is the dimensionless strain rate,  $\dot{\epsilon}$  is the strain rate,  $\text{s}^{-1}$ ;  $\dot{\epsilon}_0$  is the reference strain rate,  $\text{s}^{-1}$ .  $T^* = (T - T_{\text{ref}})/(T_m - T_{\text{ref}})$  is the relative temperature,  $T$  is the absolute temperature, K;  $T_m$  is the melting temperature (1757 K for 35CrMo steel) and  $T_{\text{ref}}$  is the reference temperature, K.

In Equation (1), the first item  $(A + B\epsilon^n)$  plays a leading role in the predicted result and determines the approximate range of stress. The  $(1 + C \ln \dot{\epsilon}^*)$  of second item and  $(1 - T^{*m})$  of third item at reference strain rate and reference temperature equal to 1, and do not affect the calculation results, but they will play an adjustment role in the calculation of flow stress when the temperature and strain rate deviate from the reference point. The strain rate sensitivity coefficient  $C$  and thermal softening exponent  $m$  determine the magnitude of the adjustment.

Compared with Arrhenius equation, JC constitutive equation has the characteristic of simple parameters. It is used to predict the rheological behavior of the material with little change in the flow stress after the peak stress, but the prediction effect is not ideal for the complex rheological behavior of those materials [35,47,48]. It is found that the second order polynomial can more accurately describe the relationship between flow stress and strain, rather than the original exponential expression. Furthermore, the item  $(1 - T^{*m})$  can be rewritten as an exponential relationship between  $\sigma$  and  $(T - T_{\text{ref}})$ . Therefore, a modified JC model is proposed with the following form:

$$\sigma = \left(A_1 + B_1\epsilon + B_2\epsilon^2\right) \left(1 + C_0 \ln \dot{\epsilon}^*\right) \exp \left[ \left(\lambda_1 + \lambda_2 \ln \dot{\epsilon}^*\right) (T - T_{\text{ref}}) \right] \quad (2)$$

where  $A_1$ ,  $B_1$ ,  $B_2$ ,  $C_0$ ,  $\lambda_1$ , and  $\lambda_2$  are the JC model parameters, the meanings of  $\sigma$ ,  $\epsilon$ ,  $T$ ,  $T_{\text{ref}}$  and  $\dot{\epsilon}^*$  are the same as that of the original JC model.

### 4. Results and Discussion

#### 4.1. The Modified JC Model

When the deformation conditions at reference temperature 1123 K and strain rate  $0.1 \text{ s}^{-1}$ , Equation (2) is transformed to:

$$\sigma = (A_1 + B_1\varepsilon + B_2\varepsilon^2) \tag{3}$$

Substitute stress and strain data (from 0.25 to 0.6) under the deformation conditions, the  $\sigma$ - $\varepsilon$  curve can be obtained, and conduct two-order polynomial fitting. Then, the values of  $A_1$ ,  $B_1$ , and  $B_2$  can be fitted as 114.45 MPa, 227.75 MPa, and 197.47 MPa, respectively, as shown in Figure 2.

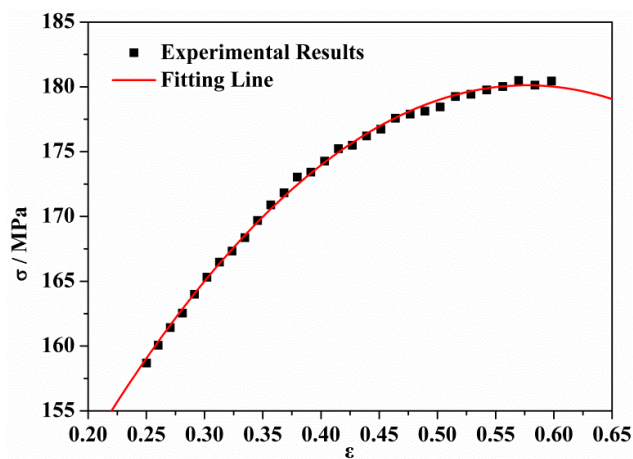


Figure 2. Relationship between  $\sigma$  and  $\varepsilon$  (1123 K/ $0.1 \text{ s}^{-1}$ ).

When the deformation temperature is 1123 K, Equation (2) can be rearranged to the following forms:

$$\frac{\sigma}{(A_1 + B_1\varepsilon + B_2\varepsilon^2)} = (1 + C_0 \ln \dot{\varepsilon}^*) \tag{4}$$

Substituting the three different strain rates and the corresponding flow stress at different strains (from 0.25 to 0.6 with the interval of 0.05, a total of eight strain values) into Equation (4), draw  $\sigma/(A_1 + B_1\varepsilon + B_2\varepsilon^2)$ - $\ln \dot{\varepsilon}^*$  curve, and carry out linear fitting, as shown in Figure 3, one gets  $C_0$  is the strain-dependent parameter, and  $C_0 = C_0(\varepsilon)$ . Then, parameter  $C_0$  corresponds to the value of the different strains as shown in Table 1.

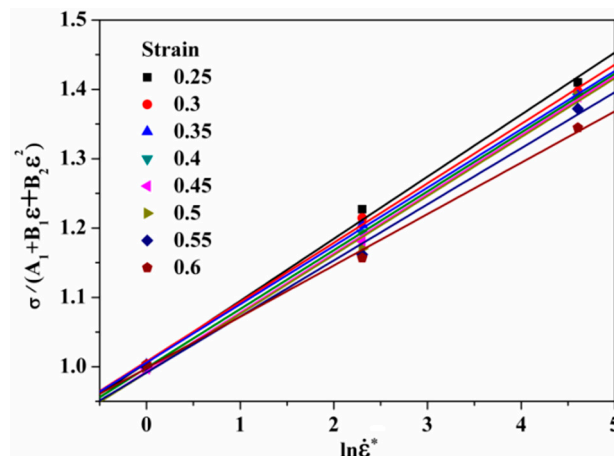
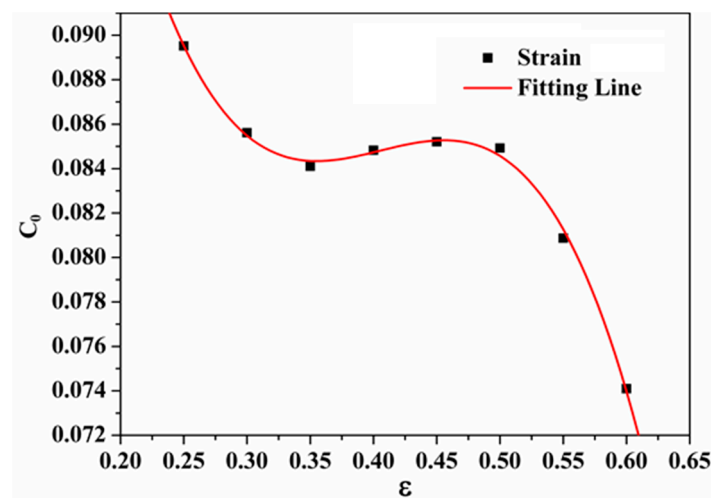


Figure 3. Relationship between  $\sigma/(A_1 + B_1\varepsilon + B_2\varepsilon^2)$  and  $\ln \dot{\varepsilon}^*$  to determine material parameter  $C_0$ .

**Table 1.** Parameter  $C_0$  corresponds to the value of the different strains.

$\varepsilon$	0.25	0.30	0.35	0.40	0.45	0.50	0.55	0.60
$C_0$	0.08952	0.08562	0.08411	0.08483	0.08521	0.08493	0.08087	0.0741

Fitting the relationship between  $C_0$  and  $\varepsilon$ , we can find that the  $C_0$  value is a cubic function of strain,  $C_0 = C_1 + C_2\varepsilon + C_3\varepsilon^2 + C_4\varepsilon^3$ , and the values of parameters  $C_1$ ,  $C_2$ ,  $C_3$ , and  $C_4$  can be fitted as 0.2017,  $-0.89301$ , 2.23743, and  $-1.8398$ , respectively, as shown in Figure 4. Huang et al. [45] shows that the dynamic recrystallization degree of 35CrMo steel is different under certain deformation conditions with the increase of strain. It is speculated that the strain dependency of parameter  $C_0$  may be the result of competition between strain hardening and dynamic recrystallization or dynamic recovery during hot deformation.

**Figure 4.** Relationship between  $C_0$  and  $\varepsilon$  to determine parameters  $C_1$ ,  $C_2$ ,  $C_3$ , and  $C_4$ .

Similarly, as a function of  $\lambda_1$  and  $\lambda_2$ , the strain rate related parameter  $\lambda$  is introduced, and  $\lambda$  is equal to  $\lambda_1 + \lambda_2 \ln \dot{\varepsilon}^*$ . Then, Equation (2) can be transformed as follows:

$$\frac{\sigma}{(A_1 + B_1\varepsilon + B_2\varepsilon^2)(1 + C_0 \ln \dot{\varepsilon}^*)} = e^{\lambda(T - T_{\text{ref}})} \quad (5)$$

Taking the natural logarithm on both sides of Equation (5) and one gets:

$$\ln \left[ \frac{\sigma}{(A_1 + B_1\varepsilon + B_2\varepsilon^2)(1 + C_0 \ln \dot{\varepsilon}^*)} \right] = \lambda(T - T_{\text{ref}}) \quad (6)$$

At four deformation temperatures of 1123, 1223, 1323, 1423 K, and three strain rates of 0.1, 1,  $10 \text{ s}^{-1}$ , the stress values correspond to the above mentioned eight strains. The relationships between  $\ln \left\{ \sigma / \left[ (A_1 + B_1\varepsilon + B_2\varepsilon^2)(1 + C_0 \ln \dot{\varepsilon}^*) \right] \right\}$  and  $(T - T_{\text{ref}})$  can be obtained, as shown in Figure 5. Then,  $\lambda_{(\dot{\varepsilon}^*=1)}$ ,  $\lambda_{(\dot{\varepsilon}^*=10)}$ , and  $\lambda_{(\dot{\varepsilon}^*=100)}$  can be linear fitted as  $-0.00429$ ,  $-0.00339$ , and  $-0.00268$ , respectively, when the dimensionless strain rates ( $\dot{\varepsilon}^*$ ) are 1 (Figure 5a), 10 (Figure 5b), and 100 (Figure 5c). Draw  $\lambda - \ln \dot{\varepsilon}^*$  curve, and conduct linear fitting, as shown in Figure 6, one gains  $\lambda_1 = -0.00426 \text{ K}^{-1}$  and  $\lambda_2 = 0.000349607 \text{ K}^{-1}$ .

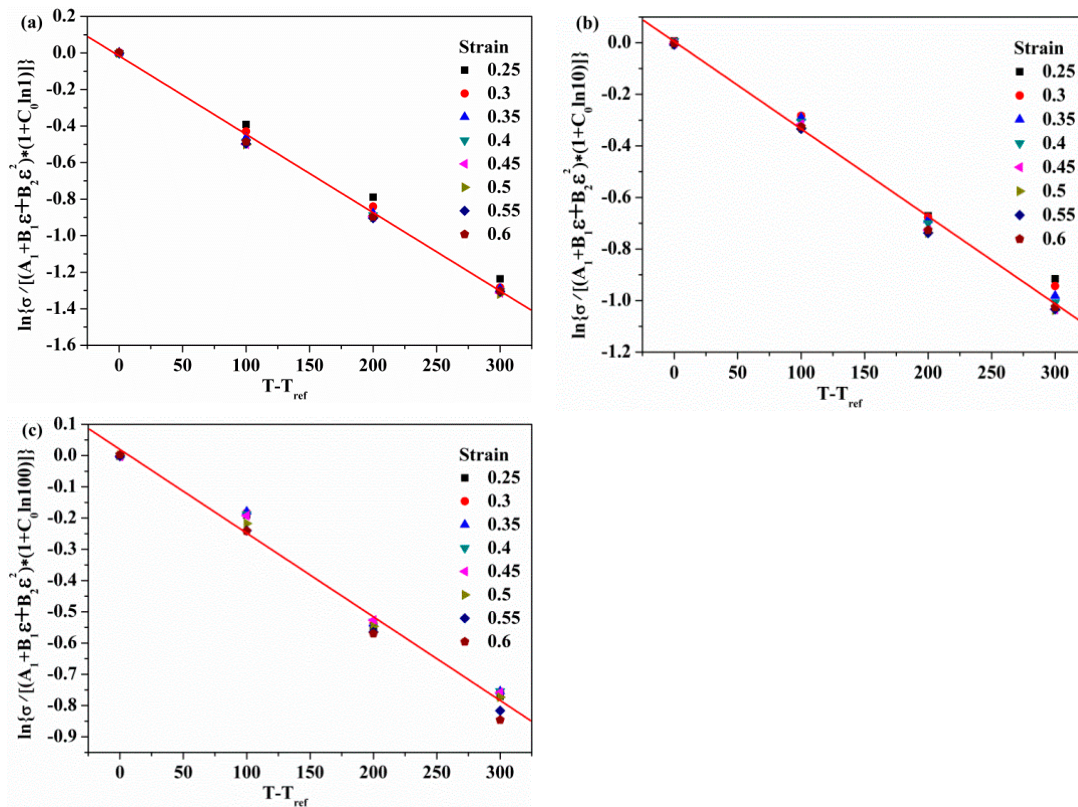


**Figure 5.** Relationships between  $\ln\left\{\frac{\sigma}{[(A_1 + B_1\varepsilon + B_2\varepsilon^2)(1 + C_0 \ln \varepsilon^*)]}\right\}$  and  $(T - T_{ref})$  for different strain rates: (a)  $\dot{\varepsilon}^* = 1$ ; (b)  $\dot{\varepsilon}^* = 10$ ; (c)  $\dot{\varepsilon}^* = 100$ .

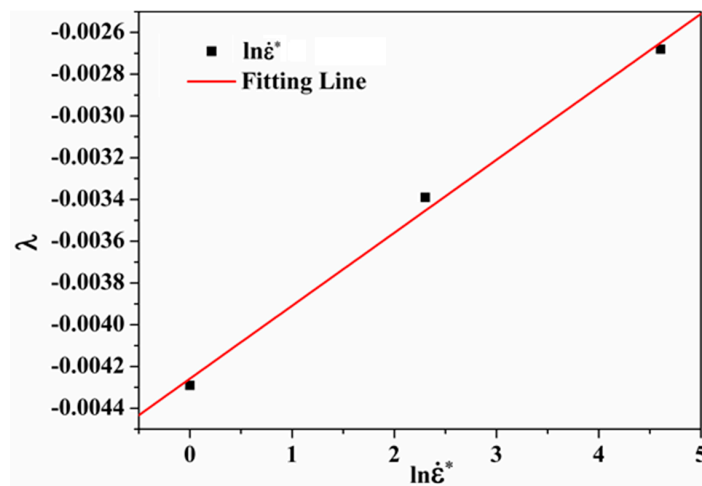


**Figure 6.** Relationship between  $\lambda$  and  $\ln \dot{\varepsilon}^*$  to determine parameters  $\lambda_1$  and  $\lambda_2$ .

The results of the modified JC model parameters are shown in Table 2. According to the parameters, calculated the predicted flow stress value, and compared with the experimental results, as shown in Figure 7.

**Table 2.** Parameters for modified JC (Johnson-Cook) equation for 35CrMo steel.

Parameters	$A_1$	$B_1$	$B_2$	$C_1$	$C_2$	$C_3$	$C_4$	$\lambda_1$	$\lambda_2$
Value	114.45	227.75	197.47	0.2017	-0.89301	2.23743	-1.8398	-0.00426	0.000349607

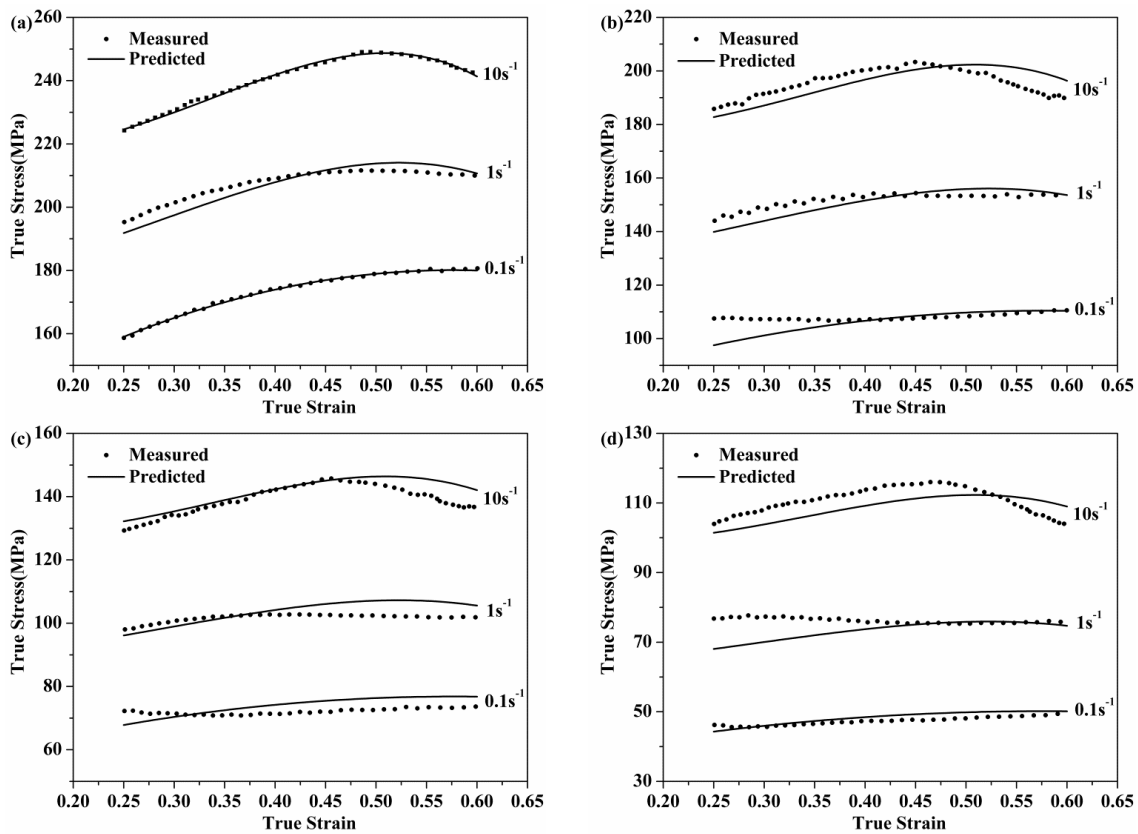


**Figure 7.** The comparison of the model predictions with experimental results at various temperatures and strain rates: (a) 1123 K; (b) 1223 K; (c) 1323 K and (d) 1423 K.

#### 4.2. Error Analysis of Prediction Results

As shown in Figure 7, it can be observed that the predicted value is in good agreement with the experimental data in most compression conditions. The correlation coefficient ( $R$ ) is a commonly used statistic can represent the strength of linear relationship between experimental and the predicted values. It should be noted that the higher value of  $R$  may not necessarily indicate a better degree of compliance since the model tends to be higher or lower. Therefore, it is necessary to introduce the average absolute error ( $\Delta$ ) to represent the deviation of the predicted values from the experimental data. The mathematical expressions are:

$$R = \frac{\sum_{i=1}^N (\sigma_{\text{exp}}^i - \bar{\sigma}_{\text{exp}}) (\sigma_{\text{p}}^i - \bar{\sigma}_{\text{p}})}{\sqrt{\sum_{i=1}^N (\sigma_{\text{exp}}^i - \bar{\sigma}_{\text{exp}})^2 \sum_{i=1}^N (\sigma_{\text{p}}^i - \bar{\sigma}_{\text{p}})^2}} \quad (7)$$

$$\Delta = \frac{1}{N} \sum_{i=1}^N \left| \frac{\sigma_{\text{exp}}^i - \sigma_{\text{p}}^i}{\sigma_{\text{exp}}^i} \right| \times 100\% \quad (8)$$

where  $\bar{\sigma}_{\text{exp}}$  and  $\bar{\sigma}_{\text{p}}$  are the mean values of  $\sigma_{\text{exp}}$  (Experimental measured flow stress values) and  $\sigma_{\text{p}}$  (Model prediction values), respectively,  $N$  is the total number of observation points. The  $R$  between the experimental and predicted data from modified JC model is 0.99683 (Figure 8), and the  $\Delta$  for entire ranges is 2.22%. The results show that the modified JC model can accurately and estimate the flow stress of 35CrMo steel and can be used to analyze the problem in forming process.

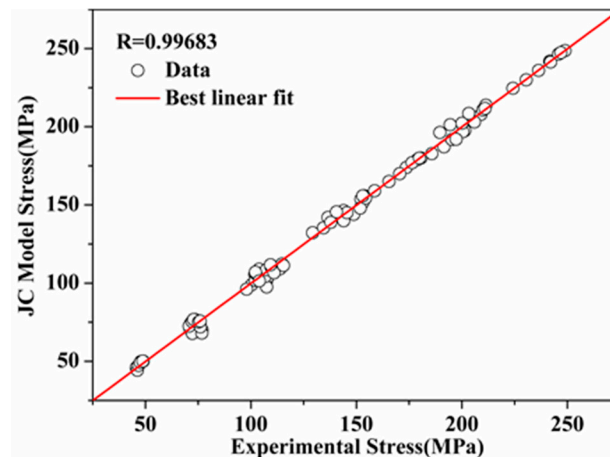


**Figure 8.** Correlation coefficient between the modified JC model and experiment data over the entire range of strains (0.25–0.6 in steps of 0.05), temperatures (1123–1423 K), and strain rates ( $0.1\text{--}10\text{ s}^{-1}$ ).

## 5. Conclusions

In this study, a uniaxial compression experimental program is carried out over a wide range of temperatures (1123–1423 K) and strain rates ( $0.1\text{--}10\text{ s}^{-1}$ ) to obtain the flow behavior of 35CrMo steel. The results show that under low temperature and high strain rate, the strain hardening effect is stronger than the dynamic recrystallization softening effect and the true stress-strain curves continues to rise. At high temperature and low strain rate, the stress increased rapidly to the peak after a slight decline, and followed by a steady state flow. This indicates that the strain hardening and recrystallization behavior of 35CrMo steel is affected by temperature, strain, and strain rate, and its true stress-strain curves can be observed typical work hardening and dynamic softening features. Accordingly, a modified JC model was developed, and its prediction results agree well with the experimental results at the selected temperatures and strain rates. The correlation of the predicted value is 0.9968, and the absolute error is about 2.22%.

**Acknowledgments:** The authors are grateful for the financial supported by the Fundamental Research Funds for the Central Universities of Central South University (2017zzts645) and the National Program on Key Basic Research Project of China (2014CB046702).

**Author Contributions:** Zhengbing Xiao and Sanxing Wang conceived and designed the experiments; Zhengbing Xiao, Hui Liu, and Sanxing Wang performed the experiments; Sanxing Wang analyzed the data; Yuanchun Huang and Yu Liu contributed reagents, materials, and analysis tools; and Sanxing Wang wrote the paper.

**Conflicts of Interest:** The authors declare no conflict of interest.

## References

1. Yue, W.; Sun, X.; Wang, C.; Fu, Z.; Liu, Y.; Liu, J. A comparative study on the tribological behaviors of nitrated and sulfur-nitrated 35CrMo steel lubricated in PAO base oil with MoDTC additive. *Tribol. Int.* **2011**, *44*, 2029–2034. [[CrossRef](#)]
2. Zhang, J.W.; Lu, L.T.; Shiozawa, K.; Zhou, W.N.; Zhang, W.H. Effect of nitrocarburizing and post-oxidation on fatigue behavior of 35CrMo alloy steel in very high cycle fatigue regime. *Int. J. Fatigue* **2011**, *33*, 880–886. [[CrossRef](#)]
3. Zhang, J.W.; Lu, L.T.; Wu, P.B.; Ma, J.J.; Wang, G.G.; Zhang, W.H. Inclusion size evaluation and fatigue strength analysis of 35CrMo alloy railway axle steel. *Mater. Sci. Eng. A* **2013**, *562*, 211–217. [[CrossRef](#)]
4. Xiao, Z.B.; Huang, Y.C.; Liu, Y. Plastic deformation behavior and processing maps of 35CrMo steel. *J. Mater. Eng. Perform.* **2016**, *25*, 1219–1227. [[CrossRef](#)]
5. Liang, G.; Shi, C.; Zhou, Y.; Mao, D. Effect of ultrasonic treatment on the solidification microstructure of die-cast 35CrMo steel. *Metals* **2016**, *6*, 260. [[CrossRef](#)]

6. Tavares, S.S.M.; Pardal, J.M.; Ponzio, E.; Loureiro, A.; De Souza, J.A. Influence of microstructure on the corrosion resistance of hyperduplex stainless steel. *Mater. Corros.* **2015**, *61*, 313–317. [[CrossRef](#)]
7. Moura, V.S.; Lima, L.D.; Pardal, J.M.; Kina, A.Y.; Corte, R.R.A.; Tavares, S.S.M. Influence of microstructure on the corrosion resistance of the duplex stainless steel UNS S31803. *Mater. Charact.* **2008**, *59*, 1127–1132. [[CrossRef](#)]
8. Johnson, G.; Cook, W. A Constitutive Model and Data for Metals Subjected to Large Strains, High Strain Rates and High Temperatures. In Proceedings of the 7th International Symposium on Ballistics, The Hague, The Netherlands, 19–21 April 1983; pp. 541–547.
9. Johnson, G.R.; Cook, W.H. Fracture characteristics of three metals subjected to various strains, strain rates, temperatures and pressures. *Eng. Fract. Mech.* **1985**, *21*, 31–48. [[CrossRef](#)]
10. Zener, C.; Hollomon, J.H. Effect of strain rate upon plastic flow of steel. *J. Appl. Phys.* **1944**, *15*, 22–32. [[CrossRef](#)]
11. Sellars, C.M.; Mctegart, W.J. On the mechanism of hot deformation. *Acta Metall.* **1966**, *14*, 1136–1138. [[CrossRef](#)]
12. Lin, Y.C.; Liu, G. A new mathematical model for predicting flow stress of typical high-strength alloy steel at elevated high temperature. *Comput. Mater. Sci.* **2010**, *48*, 54–58. [[CrossRef](#)]
13. Haghdadi, N.; Zarei-Hanzaki, A.; Abedi, H.R. The flow behavior modeling of cast A356 aluminum alloy at elevated temperatures considering the effect of strain. *Mater. Sci. Eng. A* **2012**, *535*, 252–257. [[CrossRef](#)]
14. Yin, F.; Hua, L.; Mao, H.; Han, X. Constitutive modeling for flow behavior of GCr15 steel under hot compression experiments. *Mater. Des.* **2013**, *43*, 393–401. [[CrossRef](#)]
15. Haj, M.; Mansouri, H.; Vafaei, R.; Ebrahimi, G.R.; Kanani, A. Hot compression deformation behavior of AISI 321 austenitic stainless steel. *Int. J. Miner. Metall. Mater.* **2013**, *20*, 529–534. [[CrossRef](#)]
16. Zou, D.N.; Wu, K.; Han, Y.; Zhang, W.; Cheng, B.; Qiao, G.J. Deformation characteristic and prediction of flow stress for as-cast 21Cr economical duplex stainless steel under hot compression. *Mater. Des.* **2013**, *51*, 975–982. [[CrossRef](#)]
17. Wu, H.Y.; Zhu, F.J.; Wang, S.C.; Wang, W.R.; Wang, C.C.; Chiu, C.H. Hot deformation characteristics and strain-dependent constitutive analysis of Inconel 600 superalloy. *J. Mater. Sci.* **2012**, *47*, 3971–3981. [[CrossRef](#)]
18. Samantaray, D.; Phaniraj, C.; Mandal, S.; Bhaduri, A.K. Strain dependent rate equation to predict elevated temperature flow behavior of modified 9Cr-1Mo (P91) steel. *Mater. Sci. Eng. A* **2011**, *528*, 1071–1077. [[CrossRef](#)]
19. Li, H.Y.; Wei, D.D.; Li, Y.H.; Wang, X.F. Application of artificial neural network and constitutive equations to describe the hot compressive behavior of 28CrMnMoV steel. *Mater. Des.* **2012**, *35*, 557–562. [[CrossRef](#)]
20. Fazilat, H.; Ghatband, M.; Mazinani, S.; Asadi, Z.A.; Shiri, M.E.; Kalae, M.R. Predicting the mechanical properties of glass fiber reinforced polymers via artificial neural network and adaptive neuro-fuzzy inference system. *Comput. Mater. Sci.* **2012**, *58*, 31–37. [[CrossRef](#)]
21. Haghdadi, N.; Zarei-Hanzaki, A.; Khalesian, A.R.; Abedi, H.R. Artificial neural network modeling to predict the hot deformation behavior of an A356 aluminum alloy. *Mater. Des.* **2013**, *49*, 386–391. [[CrossRef](#)]
22. Lin, Y.C.; Zhang, J.; Zhong, J. Application of neural networks to predict the elevated temperature flow behavior of a low alloy steel. *Comput. Mater. Sci.* **2008**, *43*, 752–758. [[CrossRef](#)]
23. Lin, Y.C.; Chen, M.S.; Zhong, J. Prediction of 42CrMo steel flow stress at high temperature and strain rate. *Mech. Res. Commun.* **2008**, *35*, 142–150. [[CrossRef](#)]
24. Zerilli, F.J.; Armstrong, R.W. Dislocation-mechanics-based constitutive relations for material dynamics calculations. *J. Appl. Phys.* **1987**, *61*, 1816–1825. [[CrossRef](#)]
25. Chiou, S.T.; Cheng, W.C.; Lee, W.S. Strain rate effects on the mechanical properties of a Fe-Mn-Al alloy under dynamic impact deformations. *Mater. Sci. Eng. A* **2005**, *392*, 156–162. [[CrossRef](#)]
26. Follansbee, P.S.; Kocks, U.F. A constitutive description of the deformation of copper based on the use of the mechanical threshold stress as an internal state variable. *Acta Metall.* **1988**, *36*, 81–93. [[CrossRef](#)]
27. Goetz, R.L.; Seetharaman, V. Modeling dynamic recrystallization using cellular automata. *Scr. Mater.* **1998**, *38*, 405–413. [[CrossRef](#)]
28. Bodner, S.R.; Partom, Y. Constitutive equations for elastic-viscoplastic strain-hardening materials. *J. Appl. Mech.* **1975**, *42*, 385–389. [[CrossRef](#)]
29. Donahue, E.G.; Odette, G.R.; Lucas, G.E. A physically based constitutive model for a V-4Cr-4Ti alloy. *J. Nucl. Mater.* **2000**, *283–287*, 637–641. [[CrossRef](#)]

30. Wei, H.L.; Liu, G.Q.; Zhang, M.H. Physically based constitutive analysis to predict flow stress of medium carbon and vanadium microalloyed steels. *Mater. Sci. Eng. A* **2014**, *602*, 127–133. [[CrossRef](#)]
31. Mirzadeh, H. A comparative study on the hot flow stress of Mg-Al-Zn magnesium alloys using a simple physically-based approach. *J. Magnes. Alloys* **2014**, *2*, 225–229. [[CrossRef](#)]
32. Dorogoy, A.; Rittel, D. Determination of the Johnson–Cook material parameters using the SCS specimen. *Exp. Mech.* **2009**, *49*, 881–885. [[CrossRef](#)]
33. Prawoto, Y.; Fanone, M.; Shahedi, S.; Ismail, M.S.; Nik, W.B.W. Computational approach using Johnson–Cook model on dual phase steel. *Comput. Mater. Sci.* **2012**, *54*, 48–55. [[CrossRef](#)]
34. Wang, Y.P.; Han, C.J.; Wang, C.; Li, S.K. A modified Johnson–Cook model for 30Cr2Ni4MoV rotor steel over a wide range of temperature and strain rate. *J. Mater. Sci.* **2011**, *46*, 2922–2927. [[CrossRef](#)]
35. Lin, Y.C.; Chen, X.; Liu, G. A modified Johnson–Cook model for tensile behaviors of typical high-strength alloy steel. *Mater. Sci. Eng. A* **2010**, *527*, 6980–6986. [[CrossRef](#)]
36. He, A.; Xie, G.; Zhang, H.; Wang, X. A comparative study on Johnson–Cook, modified Johnson–Cook and Arrhenius-type constitutive models to predict the high temperature flow stress in 20CrMo alloy steel. *Mater. Des.* **2013**, *52*, 677–685. [[CrossRef](#)]
37. Song, W.; Ning, J.; Mao, X.; Tang, H. A modified Johnson–Cook model for titanium matrix composites reinforced with titanium carbide particles at elevated temperatures. *Mater. Sci. Eng. A* **2013**, *576*, 280–289. [[CrossRef](#)]
38. Li, H.; He, L.; Zhao, G.; Zhang, L. Constitutive relationships of hot stamping boron steel B1500HS based on the modified Arrhenius and Johnson–Cook model. *Mater. Sci. Eng. A* **2013**, *580*, 330–348. [[CrossRef](#)]
39. Umbrello, D.; M'Saoubi, R.; Outeiro, J.C. The influence of Johnson–Cook material constants on finite element simulation of machining of AISI 316L steel. *Int. J. Mach. Tools Manuf.* **2007**, *47*, 462–470. [[CrossRef](#)]
40. Bobbili, R.; Madhu, V. Effect of strain rate and stress triaxiality on tensile behavior of Titanium alloy Ti-10-2-3 at elevated temperatures. *Mater. Sci. Eng. A* **2016**, *667*, 33–41. [[CrossRef](#)]
41. Zhang, D.N.; Shangguan, Q.Q.; Xie, C.J.; Liu, F. A modified Johnson–Cook model of dynamic tensile behaviors for 7075-T6 aluminum alloy. *J. Alloys Compd.* **2015**, *619*, 186–194. [[CrossRef](#)]
42. Wang, J.; Chen, J.; Zhang, B.; Zhao, Z.; Ruan, X.Y. The flow stress model of 35CrMo structural steel during hot forming. *J. Shanghai Jiaotong Univ.* **2005**, *39*, 1784–1791.
43. Zhang, B.; Zhang, H.B.; Ruan, X.Y.; Zhang, Y. Hot deformation behavior and dynamic recrystallization model of 35CrMo steel. *Acta Metall. Sin.* **2003**, *16*, 183–191.
44. Joshi, M.; Mason, T.D. Effect of initial microstructure on plastic flow behaviour during isothermal forging of Ti-10V-2Fe-3Al. *Mater. Sci. Eng. A* **2009**, *501*, 248–254.
45. Huang, Y.; Wang, S.; Xiao, Z.; Liu, H. Critical condition of dynamic recrystallization in 35CrMo steel. *Metals* **2017**, *7*, 161. [[CrossRef](#)]
46. Lin, Y.C.; Chen, M.S.; Zhong, J. Constitutive modeling for elevated temperature flow behavior of 42CrMo steel. *Comput. Mater. Sci.* **2008**, *42*, 470–477. [[CrossRef](#)]
47. Tan, J.Q.; Zhan, M.; Liu, S.; Huang, T.; Guo, J.; Yang, H. A modified Johnson–Cook model for tensile flow behaviors of 7050-T7451 aluminum alloy at high strain rates. *Mater. Sci. Eng. A* **2015**, *631*, 214–219. [[CrossRef](#)]
48. Sun, Y.; Ye, W.H.; Hu, L.X. Constitutive modeling of high-temperature flow behavior of Al-0.62Mg-0.73Si aluminum alloy. *J. Mater. Eng. Perform.* **2016**, *25*, 1621–1630. [[CrossRef](#)]

